Sulfatides are endogenous ligands for the TLR4–MD-2 complex

Lijing Su[a,b,1,2], Muhammad Athamna[c,d,1], Ying Wang[a], Junmei Wang[e], Marina Freudenberg[f,g], Tao Yue[a], Jianhui Wang[a], Eva Marie Y. Moresco[a], Haoming He[c], Tsaffrir Zor[c,2], and Bruce Beutler[a,2]

[a]Center for the Genetics of Host Defense, University of Texas Southwestern Medical Center, Dallas, TX 75390; [b]Department of Biophysics, University of Texas Southwestern Medical Center, Dallas, TX 75390; [c]Department of Biochemistry & Molecular Biology, School of Neurobiology, Biochemistry & Biophysics, Tel Aviv University, Tel Aviv 69978, Israel; [d]Triangle Regional Research and Development Center, Kfar Qari' 3007500, Israel; [e]Department of Pharmaceutical Sciences, School of Pharmacy, University of Pittsburgh, Pittsburgh, PA 15261; [f]BIOSS Centre for Biological Signalling Studies, University of Freiburg, 79104 Freiburg, Germany; and [g]Department of Pneumology, Medical Center and Faculty of Medicine, University of Freiburg, 79106 Freiburg, Germany

Edited by K. Christopher Garcia, Stanford University, Stanford, CA, and approved June 14, 2021 (received for review March 23, 2021)

Many endogenous molecules, mostly proteins, purportedly activate the Toll-like receptor 4 (TLR4)–myeloid differentiation factor-2 (MD-2) complex, the innate immune receptor for lipopolysaccharide (LPS) derived from gram-negative bacteria. However, there is no structural evidence supporting direct TLR4–MD-2 activation by endogenous ligands. Sulfatides (3-*O*-sulfogalactosylceramides) are natural, abundant sulfated glycolipids that have variously been shown to initiate or suppress inflammatory responses. We show here that short fatty acid (FA) chain sulfatides directly activate mouse TLR4–MD-2 independent of CD14, trigger MyD88- and TRIF-dependent signaling, and stimulate tumor necrosis factor α (TNFα) and type I interferon (IFN) production in mouse macrophages. In contrast to the agonist activity toward the mouse receptor, the tested sulfatides antagonize TLR4–MD-2 activation by LPS in human macrophage-like cells. The agonistic and antagonistic activities of sulfatides require the presence of the sulfate group and are inversely related to the FA chain length. The crystal structure of mouse TLR4–MD-2 in complex with C16-sulfatide revealed that three C16-sulfatide molecules bound to the MD-2 hydrophobic pocket and induced an active dimer conformation of the receptor complex similar to that induced by LPS or lipid A. The three C16-sulfatide molecules partially mimicked the detailed interactions of lipid A to achieve receptor activation. Our results suggest that sulfatides may mediate sterile inflammation or suppress LPS-stimulated inflammation, and that additional endogenous negatively charged lipids with up to six lipid chains of limited length might also bind to TLR4–MD-2 and activate or inhibit this complex.

innate immunity | autoimmunity | Toll-like receptor | endogenous ligand | X-ray crystallography

The Toll-like receptors (TLRs) constitute a critical microbe-sensing system in mammals, detecting components of viruses, bacteria, fungi, and protozoa. TLRs are single-pass transmembrane proteins located within the plasma or endosomal membranes of innate immune cells, such as macrophages. They respond to ligand engagement by forming signaling-competent homo- or heterodimers. The three-dimensional structures of all known TLR extracellular domains share a common horseshoe-shaped structure that contains 16 to 28 leucine-rich repeats, which are responsible for ligand recognition. Ligands display distinct modes of binding to each TLR, but all induce dimerization by simultaneously interacting with the ectodomains of two different receptor chains, bringing the intracellular TIR domains into proximity, thus permitting downstream signaling (1). The active receptor dimers recruit adaptors that propagate signals ultimately leading to nuclear factor κB (NF-κB)– and/or interferon regulatory factor–dependent transcription of hundreds of genes. Important transcriptional targets include genes encoding proinflammatory cytokines such as tumor necrosis factor α (TNFα), interleukin-1β (IL-1β), and IL-6, as well as type I interferons (IFNs).

While essential for host defense, TLRs may also mediate sterile inflammation and autoimmunity as a result of inappropriate activation by endogenous molecules. For example, single-stranded DNA of host origin can induce activation of TLR9 (2). Less certain is the activation of receptor complexes containing TLR2 or TLR4 by endogenous molecules. Reported endogenous ligands for the TLR2/1–, TLR2/6–, and TLR4–myeloid differentiation factor-2 (MD-2) complexes include proteins, polysaccharides and proteoglycans, phospholipids, and small organic molecules (3). Where TLR4 is concerned, reported endogenous ligands include high-mobility group box 1, heat shock proteins, peptides derived from fibrinogen, and monosodium urate crystals (3). Oxidized phospholipids (4) and triglycerides have additionally been named as activators. In none of these cases have crystallographic data been developed to support cell-based studies, and therefore it is difficult to exclude the possibility that contaminating lipopolysaccharide (LPS) might actually have been the activating principle [as has been demonstrated for HSP60 (5)]. Moreover, it is also difficult to exclude the possible scenario of indirect activation (6).

We previously identified artificially synthesized small organic molecules with no structural resemblance to the classical bacterial ligands Pam3CSK4 and LPS that act as TLR2/1 (diprovocim) (7) and TLR4–MD-2 (neoseptins) (8) agonists, respectively. Seeking to

Significance

Toll-like receptor 4 (TLR4) is an innate immune receptor that initiates inflammation when activated by bacterial lipopolysaccharide. It may also be activated by endogenous host molecules, leading to autoinflammation and autoimmunity. We demonstrate that several sulfatide species, natural membrane glycolipids in mammals, are bona fide ligands for TLR4 and its coreceptor myeloid differentiation factor-2 (MD-2). Sulfatides with lipid chains containing 12 or 16 carbon atoms are agonists of mouse TLR4 and antagonists of human TLR4. We determined the crystal structure of the mouse TLR4–MD-2 extracellular domain in complex with C16-sulfatide at 2.1-Å resolution, providing definitive evidence of direct interaction. Structure–activity relationship studies suggest a structural basis for the differential effects of sulfatides interacting with human and mouse receptors.

Author contributions: L.S., M.A., Y.W., Junmei Wang, M.F., T.Z., and B.B. designed research; L.S., M.A., Y.W., Junmei Wang, T.Y., Jianhui Wang, and H.H. performed research; Junmei Wang contributed new reagents/analytic tools; L.S., M.A., Y.W., H.H., and T.Z. analyzed data; and L.S., M.A., Junmei Wang, E.M.Y.M., T.Z., and B.B. wrote the paper.

The authors declare no competing interest.

This article is a PNAS Direct Submission.

[1]L.S. and M.A. contributed equally to this work.

[2]To whom correspondence may be addressed. Email: lijing.su@utsouthwestern.edu, tsaffyz@tauex.tau.ac.il, or bruce.beutler@utsouthwestern.edu.

This article contains supporting information online at https://www.pnas.org/lookup/suppl/doi:10.1073/pnas.2105316118/-/DCSupplemental.

Published July 21, 2021.

determine whether endogenous molecules might indeed be TLR4–MD-2 agonists as well, we investigated the interaction between the TLR4–MD-2 complex and 3-*O*-sulfogalactosylceramides (hereafter sulfatides), endogenous glycosphingolipids that display structural similarity to lipid A, the toxic moiety of LPS recognized by TLR4–MD-2.

Unlike lipid A molecules, sulfatides contain only two hydrophobic chains, as in the parent sphingolipid ceramide. One chain is contributed by sphingosine, most commonly 18 carbon atoms in length, with a single double bond (d18:1), hydroxyl, and a C2 amino group which is acylated by a fatty acid (FA) of variable chain length, hydroxylation, and saturation. In mammalian cells, ceramide is galactosylated by ceramide galactosyltransferase to yield galactosylceramide. Finally, cerebroside sulfotransferase (CST) yields a mature sulfatide molecule bearing a negatively charged sulfate group at the 3-*O* position (Fig. 1*A*). Degradation of sulfatide is carried out by the enzymatic activity of arylsulfatase A (ASA), which requires saposin-B, a protein that extracts sulfatide from the membrane (9).

Sulfatides are present in all eukaryotic cell membranes and are particularly abundant in myelin sheaths of nerve fibers, in islet of Langerhans pancreatic cells, and in kidney cells. They are also present in mammalian plasma or serum (10–12). Several reports have indicated that sulfatides play a role in autoimmunity or inflammation, although conflicting data exist on whether they promote or inhibit it. The accumulation of sulfatides due to ASA deficiency leads to the lysosome storage disease metachromatic leukodystrophy, characterized by progressive demyelination (9). The levels of plasma sulfatides (C18:0 and C24:1) have been reported to correlate with disease status in relapsing–remitting multiple sclerosis (MS) (13), and sulfatide antibodies were detected at elevated levels in cerebrospinal fluid of MS patients (10, 12, 14). Mice with acute experimental autoimmune encephalitis (EAE) also produced elevated sulfatide antibodies (12). In contrast, others reported reduced disease severity of EAE in wild-type mice treated with sulfatides (15, 16). Postmortem brain tissues from Alzheimer's disease patients revealed a dramatic reduction in sulfatide levels, despite normal CST activity, thus suggesting accelerated degradation (17). Sulfatides were reported to be reduced in patients and mouse models of type 2 diabetes (18). Additionally, sulfatides are abundant in beta cells, and their administration lowered the incidence of type 1 diabetes in nonobese diabetic mice (19).

At the cellular level, high concentrations of brain-derived sulfatides reportedly stimulated cytokine expression and secretion by human monocytes, while galactosylceramides failed to do so (20). Accordingly, C18:0 and C24:1 sulfatide isoforms, but not C16:0, elevated nuclear p65 and p50 NF-κB levels in human THP-1 monocytes (21). In contrast, brain-derived sulfatides were shown to prevent LPS-induced TNFα production and acute lethality in mice and LPS-induced TNFα production in THP-1 cells (22). More recently, synthetic C12-sulfatide was reported to strongly stimulate TNFα and other proinflammatory cytokines through activation of NF-κB and mitogen-activated protein (MAP) kinases in rat primary microglia and astrocytes. These effects were independent of CD1d, a known receptor for sulfatides, and were partially mediated by L-selectin, which was shown to bind to sulfatide in leukocytes (23). Data also point to C24-sulfatide activation of TLR4- and TLR2-dependent signaling in human dendritic cells (24), while another report provides evidence that long FA chain sulfatides block LPS-stimulated localization of TLR4 within lipid rafts and activation of NF-κB and MAP kinases in RAW264.7 macrophages, and prevent LPS-induced acute lethality in mice (25). Thus, the role of sulfatides in inflammation and specifically in TLR binding/activation remains poorly defined.

We recognized that the lipid chains of three sulfatide molecules could potentially mimic the interactions and volume of the six acyl chains characteristically present in a single lipid A molecule; the galactose moiety could mimic the interactions made by the glucosamine units of lipid A; and the sulfate groups may mimic the interactions made by the phosphates of lipid A (Fig. 1*A*). We investigated the interactions between different subspecies of sulfatides and the TLR4–MD-2 complex using cellular, biophysical, and structural techniques.

Results

Short FA Chain Sulfatides Are Agonists in Mouse Macrophages but Antagonists in Human Macrophages. We stimulated primary mouse peritoneal macrophages or a human macrophage cell line (phorbol 12-myristate 13-acetate [PMA]–differentiated THP-1 monocytes) with lipid vesicle preparations (*SI Appendix*, Fig. S1) of C12-sulfatide (d18:1/12:0), C16-sulfatide (d18:1/16:0), C18-sulfatide (d18:1/18:0), porcine brain-derived sulfatides, or the nonsulfated C16-sulfatide precursor C16-galactosylceramide, and measured TNFα in the culture media after 4 h. LPS and lipid A served as positive controls and standards for TNFα production. Both C12- and C16-sulfatides strongly induced TNFα production by mouse peritoneal macrophages with efficacies similar to that of smooth LPS but much higher than that of lipid A, and approximate half-maximal effective concentration (EC_{50}) values of 7 and 17 μM, respectively (Fig. 1*B*). Neither C18-sulfatide nor C16-galactosylceramide (lacking the sulfate group) induced TNFα production by mouse peritoneal macrophages. Porcine brain-derived sulfatides that consist predominantly of C24-sulfatides induced extremely low TNFα concentrations (~80 pg/mL) at the highest concentration tested (100 μM) (*SI Appendix*, Fig. S2*A*). Moreover, C18-sulfatide and porcine brain-derived sulfatides were also unable to inhibit TNFα secretion by mouse peritoneal macrophages stimulated by lipid A (10 ng/mL) (*SI Appendix*, Fig. S2*A*). Consistently, C12-sulfatide strongly stimulated TNFα secretion by mouse RAW264.7 macrophages with an EC_{50} of 11 μM, while the nonsulfated precursor C12-galactosylceramide was completely inactive (*SI Appendix*, Fig. S2*B*). These results suggest that short, but not long, FA chain sulfatides are agonists for TNFα production in mice and that the negatively charged sulfate group is required for their agonistic activity.

As distinct from mouse peritoneal macrophages, human macrophage-like THP-1 cells responded only to the high concentrations of C12-sulfatide with production of very low levels of TNFα (Fig. 1*C*). However, all sulfatides tested and C16-galactosylceramide exhibited dose-dependent antagonistic activity toward lipid A–induced TNFα production in THP-1 cells (Fig. 1*D*). C12-, C16-, and C18-sulfatides fully inhibited TNFα secretion from lipid A–stimulated (5 ng/mL) THP-1 cells at concentrations equal to or greater than 12.5, 50, and 50 μM, respectively. Compared with C16-sulfatide, its precursor C16-galactosylceramide showed weak antagonistic activity toward lipid A at all concentrations tested. Interestingly, C16-sulfatide could inhibit lipid A activity better than C12-sulfatide at concentrations lower than about 10 μM. C18-sulfatide is a less potent antagonist of lipid A activity than C12- and C16-sulfatides. Porcine brain sulfatides could only partially inhibit TNFα secretion even at high concentrations, exhibiting about 21 and 57% inhibition at 50 and 100 μM, respectively. Notably, inhibition of TNFα secretion by C16-sulfatide was inversely correlated with LPS concentration, suggesting competitive inhibition (*SI Appendix*, Fig. S2*C*). These data suggest that short FA chain sulfatides compete better than long FA chain sulfatides with lipid A for binding to its receptor TLR4–MD-2, and that a sulfate group is important for this function.

Short FA Chain Sulfatide Activity Is Dependent on TLR4–MD-2 and Largely Independent of CD14. We analyzed TNFα production induced by sulfatide treatment of peritoneal macrophages isolated from wild-type C57BL/6J mice and mice deficient in TLR4 ($Tlr4^{lps3/lps3}$) or TLR2 ($Tlr2^{-/-}$), which also recognizes lipid molecules. Both LPS and C12-sulfatide induced TNFα production by wild-type or TLR2-deficient macrophages but not by TLR4-deficient

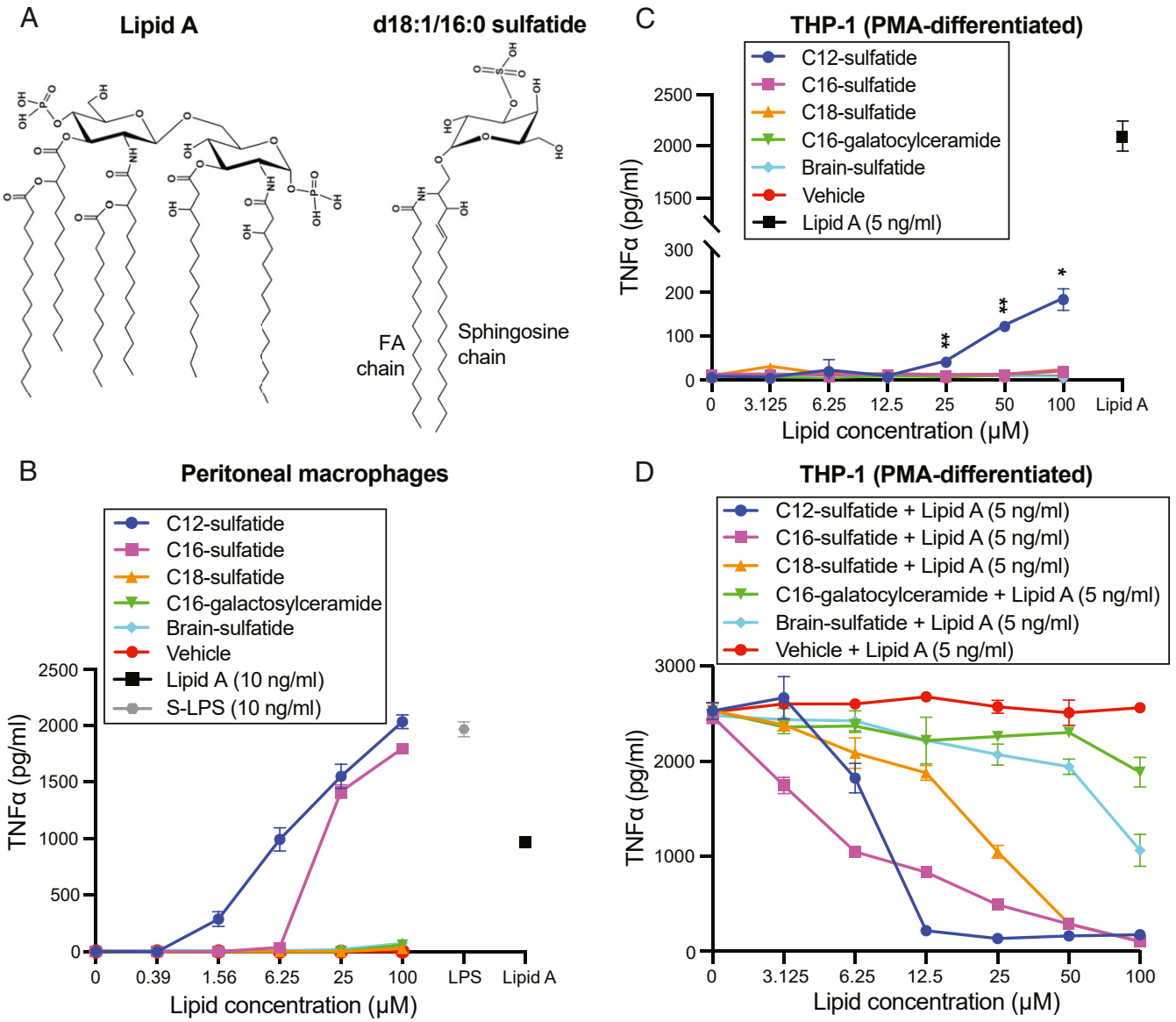

Fig. 1. TNFα production by macrophages stimulated with sulfatides. (*A*) Chemical structures of lipid A and C16-sulfatide. (*B* and *C*) TNFα in the culture media of mouse peritoneal macrophages (*B*) and PMA-differentiated human THP-1 cells (*C*) after treatment with sulfatides, C16-galactosylceramide, smooth LPS, or lipid A for 4 h; $n = 3$. $^{*}P < 0.05$, $^{**}P < 0.01$ (two-way ANOVA followed by Dunnett's posttest for comparison with the vehicle [water]-treated condition). (*D*) TNFα in the culture media of PMA-differentiated human THP-1 cells pretreated with sulfatides, C16-galactosylceramide, or vehicle (water) for 1 h, followed by addition of 5 ng/mL lipid A for another 4 h; $n = 3$. All data (mean ± SEM) are representative of at least two independent experiments.

macrophages, indicating that TLR4, but not TLR2, is necessary for the agonistic activity of C12-sulfatide (Fig. 2*A*). To address the requirement for MD-2 in the response to sulfatides, we used SW620 cells to ectopically express either TLR4 or MD-2 or both proteins. Only expression of both TLR4 and MD-2 enabled strong NF-κB reporter activation by either C12-sulfatide or LPS. Expression of TLR4 alone resulted in low but statistically significant activation by either C12-sulfatide or LPS, probably reflecting low endogenous MD-2 expression in the SW620 cells, whereas expression of MD-2 alone did not permit activation by either agonist (Fig. 2*B*). These results imply that both TLR4 and MD-2 are required for signaling leading to TNFα production induced by short FA chain sulfatides.

CD14 acts as a coreceptor with TLR4–MD-2 for detection of LPS. CD14 was proposed to bind to the acyl chains of LPS through hydrophobic interactions and deliver the bound LPS to TLR4–MD-2 (26, 27). It is required for TLR4 signaling activated by highly glycosylated LPS (smooth LPS) but not for nonglycosylated LPS-like molecules such as lipid A, nor for the non-LPS synthetic agonist neoseptin-3 (8). We found that peritoneal macrophages from CD14-deficient mice ($Cd14^{hdl/hdl}$) displayed TNFα responses similar to wild-type macrophages at the highest tested concentrations of C12-sulfatide and lipid A but moderately decreased responses to these stimuli at lower concentrations (*SI Appendix*, Fig. S3). Compared with wild-type macrophages, CD14 deficiency resulted in moderately decreased TNFα responses to C16-sulfatide at all concentrations for which a response was detected (*SI Appendix*, Fig. S3*A*). In contrast, deficiency of CD14 significantly decreased the response to higher concentrations (100 and 10 ng/mL) of smooth LPS and abolished the response to the lower concentration (1 ng/mL) (*SI Appendix*, Fig. S3*B*). These results suggest that the agonistic activity of short FA chain sulfatides in mouse peritoneal macrophages is largely CD14-independent, consistent with an assisting but not required role for CD14 in detection of non-LPS ligands.

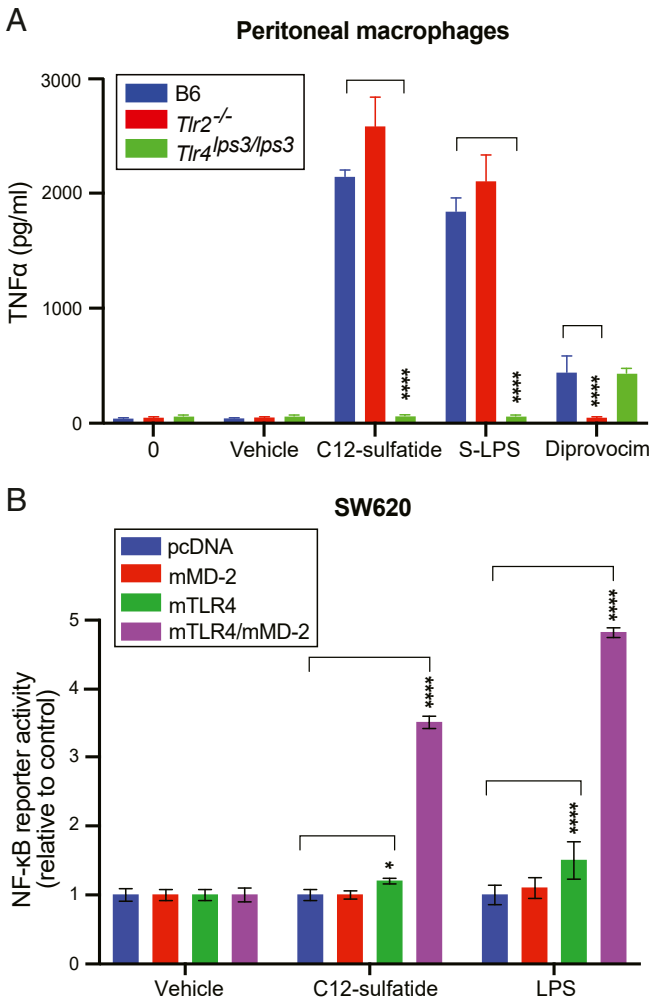

Fig. 2. Activity of short FA chain sulfatides requires mTLR4–MD-2. (*A*) TNFα in the culture media of mouse peritoneal macrophages isolated from WT (B6), *Tlr2*-knockout, or *Tlr4*-deficient mice after treatment with vehicle (water), C12-sulfatide (135 μM), smooth LPS (1 ng/mL), or diprovocim (5 μM) for 4 h; $n = 2$. (*B*) NF-κB–dependent luciferase activity in SW620 cells transiently expressing mouse TLR4, MD-2, or TLR4 plus MD-2, and stimulated with vehicle, C12-sulfatide (15 μM), or rough LPS (1 μg/mL); $n = 4$. Data were normalized against renilla luciferase activity and against activity in cells treated with vehicle (water) and expressing the same plasmid(s). Data (mean ± SEM) are representative of at least two independent experiments. $^*P < 0.05$, $^{***}P \leq 0.001$, $^{****}P \leq 0.0001$ (two-way ANOVA followed by Dunnett's posttest for comparison with the WT [B6] condition [*A*] and with the vector control [pcDNA] [*B*]).

C12-Sulfatide Activates Both MyD88- and TRIF-Dependent Signaling. NF-κB–dependent transcription in response to TLR4 agonists is activated via signaling mediated by the two adaptor proteins MyD88 and TRIF. To determine whether sulfatide employs either or both adaptors, we examined whether exposure of mouse macrophages to C12-sulfatide stimulates 1) TLR4-dependent NF-κB transcriptional activity; 2) rapid MyD88-dependent phosphorylation of the MAP kinases ERK1/2, p38, and JNK1/2 (28); and 3) TRIF-dependent expression and secretion of IFNs (29, 30). Treatment of mouse RAW264.7 macrophages with either C12-sulfatide or LPS for 4 h strongly stimulated NF-κB reporter activity (Fig. 3*A*) and TNFα secretion (*SI Appendix*, Fig. S4*A*). TAK-242, a selective TLR4 inhibitor that targets its intracellular domain, thereby blocking recruitment of MyD88 and TRIF, abolished both responses (Fig. 3*A* and *SI Appendix*, Fig. S4*A*). Treatment of bone marrow–derived macrophages (BMDMs) with C12-sulfatide (10 μM, ~EC_{50}) for 30 min increased the phosphorylation of ERK1/2, p38, and JNK1/2 by 16-, 10-, and 8-fold, respectively, compared with resting cells (Fig. 3*B* and *SI Appendix*, Fig. S4 *B–D*). LPS used at a concentration (6.5 ng/mL) slightly below its EC_{50} (9.5 ng/mL) was similarly effective in inducing ERK1/2 phosphorylation, and less effective than C12-sulfatide in inducing p38 phosphorylation (Fig. 3*B* and *SI Appendix*, Fig. S4 *B* and *C*). A significantly higher concentration of LPS (100 ng/mL) was required to stimulate JNK1/2 phosphorylation, consistent with earlier reports (31) (Fig. 3*B* and *SI Appendix*, Fig. S4*D*). C12-sulfatide and LPS were similarly efficient in induction of type I IFN activity in the BMDM conditioned medium (Fig. 3*C*). Poly(I:C), which signals exclusively via TRIF, was, as expected, more efficient in inducing type I IFN than in inducing TNFα (Fig. 3 *C* and *D*). The similarity between the responses to C12-sulfatide and LPS in these assays suggests that like LPS, C12-sulfatide activates both MyD88- and TRIF-dependent signaling.

To directly evaluate the importance of the MyD88 and TRIF adaptor proteins for TNFα induction by sulfatide, we employed BMDMs from mice deficient in either TLR4, MyD88, or TRIF, and treated them with C12-sulfatide, LPS, Pam2CKS4, or poly(I:C) for 24 h. The TNFα response to LPS was impaired in BMDMs from all knockout (KO) mice, whereas the response to the TLR2/6 agonist Pam2CSK4 was impaired only in the absence of MyD88, and the response to the TLR3 agonist poly(I:C) was impaired only in the absence of TRIF (Fig. 3*D*). TNFα production in response to C12-sulfatide was qualitatively similar to the response to LPS; the TNFα response was fully abolished in BMDMs from TLR4-KO mice, and significantly reduced in BMDMs from MyD88-KO and TRIF-KO mice. Taken together, these results suggest that C12-sulfatide stimulates proinflammatory signaling in macrophages directly via TLR4 and its adaptor proteins MyD88 and TRIF.

Sulfatides Directly Interact with Mouse TLR4–MD-2 and the FA Chain Length Is Important for Dimerizing TLR4–MD-2 for Activation. To establish whether sulfatides and TLR4–MD-2 physically interact, we analyzed the formation of TLR4–MD-2–sulfatide complexes containing purified ectodomains of mouse (m) TLR4–MD-2 using a native polyacrylamide-gel electrophoresis (PAGE) mobility-shift assay (Fig. 4*A* and *SI Appendix*, Fig. S5). This assay separates proteins based on differences in both protein size and charge. Lipid A served as a control and was compared with sulfatides in their abilities to bind and induce dimerization of mTLR4–MD-2. Unliganded (apo) mTLR–MD-2 existed in solution as a monomer (32), appearing as a doublet likely due to differential glycosylation of MD-2 (Fig. 4*A*, lane 1). mTLR4–MD-2 was partially dimerized in solution when directly mixed with lipid A, resulting in a dimer band (upper) and a monomer band (lower) following PAGE (Fig. 4*A*, lane 2). Compared with unliganded (apo) mTLR4–MD-2 (Fig. 4*A*, lane 1), the dimeric mTLR4–MD-2–lipid A complex migrated slower due to its larger size. The monomeric mTLR4–MD-2–lipid A complex migrated faster than apo mTLR4–MD-2 (Fig. 4*A*, lanes 1 and 2), likely due to the presence of two negatively charged phosphate groups from lipid A in the monomer complex.

C12-sulfatide binding resulted in dimerization of the majority of mTLR4–MD-2 in the sample (Fig. 4*A*, lane 3), as reflected by the slower migration compared with apo mTLR4–MD-2 (Fig. 4*A*, lane 1). C16-sulfatide induced dimerization of a small fraction of mTLR4–MD-2 (Fig. 4*A*, lane 4). C18-sulfatide, C16-galactosylceramide, and porcine brain-derived sulfatides did not induce dimerization of mTLR4–MD-2 (Fig. 4*A*, lanes 5, 6, and 8). Yet, C16-, C18-, and porcine brain-derived sulfatides (Fig. 4*A*, lanes 4, 5, and 8 and *SI Appendix*, Fig. S5) all induced a very small downward shift of the top thick band of monomeric mTLR4–MD-2–sulfatide relative to apo mTLR4–MD-2 (Fig. 4*A*, lanes 1, 7, and 9 and *SI Appendix*, Fig. S5), indicating formation of some mTLR4–MD-2–sulfatide monomers with these sulfatide species. This downward shift was consistently small even when high

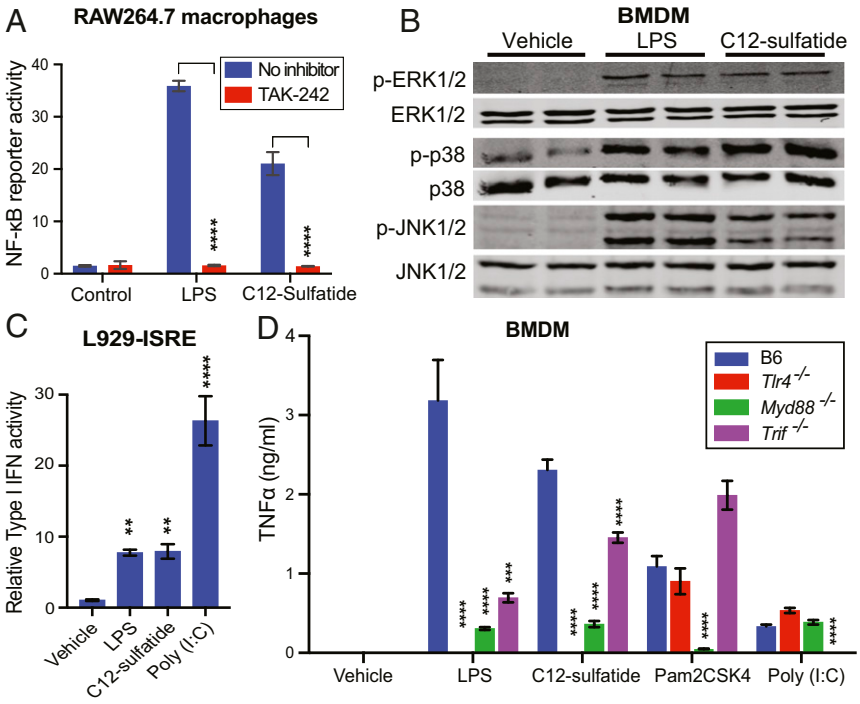

Fig. 3. C12-sulfatide activates both MyD88- and TRIF-dependent signaling. (*A*) NF-κB–dependent luciferase activity in RAW264.7 macrophages preincubated for 2 h with or without TAK-242 (0.1 μM), and then stimulated with vehicle control or EC_{50} value concentrations of C12-sulfatide (11 μM) or rough LPS (9.5 ng/mL) for 4 h; $n = 3$. Luciferase data were normalized against renilla luciferase activity and against the data measured in control cells (treated with 0.2% DMSO). $^{****}P < 0.0001$ (multiple *t* test). (*B*) Immunoblot analysis of phosphorylated (p) ERK1/2, p38, and JNK in lysates of mouse BMDMs after treatment with C12-sulfatide (10 μM) or rough LPS (6.5 ng/mL for ERK1/2 and p38 phosphorylation; 100 ng/mL for JNK1/2 phosphorylation) for 30 min. (*C*) BMDMs were treated with rough LPS (6.5 ng/mL), C12-sulfatide (10 μM), or poly(I:C) (10 μg/mL) for 24 h; $n = 3$. Type I IFN reporter activity in L929-ISRE cells stimulated for 4 h with conditioned BMDM culture media. $^{**}P < 0.01$, $^{****}P < 0.0001$ (Student's *t* test). (*D*) TNFα in the culture media of WT (B6), *Tlr4*$^{-/-}$, *Myd88*$^{-/-}$, and *Trif*$^{-/-}$ BMDMs after treatment with C12-sulfatide (10 μM), rough LPS (6.5 ng/mL), Pam2CSK4 (1 ng/mL), or poly(I:C) (10 μg/mL) for 24 h; $n = 3$. $^{***}P < 0.001$, $^{****}P < 0.0001$ (multiple *t* test). Data (mean ± SEM) are representative of at least three independent experiments.

concentrations of protein and lipid vesicles were used. In addition, the downshift of the mTLR4–MD-2–sulfatide monomer band was much smaller than that of the mTLR4–MD-2–lipid A monomer band, suggesting that fewer than three sulfatides were bound in each mTLR4–MD-2–sulfatide monomer (a −3 charge expected for three bound sulfatides should result in a similar downshift as a −4 charge of lipid A at the experimental pH of 8.3, but did not). These data indicate that C12-, C16-, C18-, and porcine brain-derived sulfatides directly bind to mTLR4–MD-2 and suggest that sulfatides with shorter FA chains were able to induce mTLR4–MD-2 dimerization better than longer FA chain sulfatides, consistent with the TNFα responses of mouse peritoneal macrophages to sulfatides with different FA chain lengths (Fig. 1*B*).

Three C16-Sulfatide Molecules Bind to the Hydrophobic Pocket of MD-2 and Induce Agonistic Dimerization of Two mTLR4–MD-2 Complexes. Because natural sulfatides in mice and humans contain FA chains with at least 14 carbons and C16-sulfatides are far more abundant than C14-sulfatides (33), we used C16-sulfatide for structural studies with mTLR4–MD-2. We determined the crystal structure of the ectodomain of the mTLR4–MD-2 heterodimer in complex with C16-sulfatide at 2.1-Å resolution (*SI Appendix*, Table S1). C16-sulfatide induced formation of an "m"-shaped dimer of the mTLR4–MD-2 heterodimers (Fig. 4*B*) similar to that observed in the previously reported structures of TLR4–MD-2 bound to agonists such as LPS, lipid A, and neoseptin-3 (8, 34). The overall conformations of the mTLR4–MD-2–C16-sulfatide dimer and the TLR4–MD-2–lipid A dimer (Protein Data Bank [PDB] ID code 5IJD) were similar, with rmsd's of about 1.5 Å between the atoms of the two structures (*SI Appendix*, Fig. S6*A*). By convention, in all structure depictions, we use an asterisk to label mTLR4 and mMD-2 in the second mTLR4–MD-2 heterodimer of the active receptor complex.

The Phe126 loop of mMD-2 is near the bound ligand and at the dimerization interface of the two mTLR4–MD-2 heterodimers (Fig. 4*B*) and has been shown to change conformation upon lipid A binding to the receptor complex (8) (Fig. 4*C*). We observed that C16-sulfatide bound to the mMD-2 hydrophobic pocket and induced a local conformational change in the Phe126 loop similar to that induced by lipid A (Fig. 4 *B* and *C*). This conformational change was also observed in other agonist-bound TLR4–MD-2 structures including LPS-, lipid IVa–, and neoseptin-3–bound mTLR4–MD-2 structures and the LPS-bound human TLR4–MD-2 structure (8, 32, 34) but not in antagonist-bound TLR4–MD-2 structures such as lipid IVa– or eritoran-bound human TLR4–MD-2 structures (35, 36). Thus, a conformational signature of TLR4–MD-2 activation was observed upon C16-sulfatide binding to the mouse receptor.

The electron density map revealed that six lipid chains (Fig. 4*D*), corresponding to three C16-sulfatide molecules, occupied the hydrophobic pocket of mMD-2 in each mTLR4–MD-2 heterodimer of the m-shaped dimer. The densities for the lipid chains inside the mMD-2 hydrophobic pocket were not as clearly defined as the densities for the polypeptide chains, likely due in large part to the flexibility of the lipid chains as well as to heterogeneity in the number of C16-sulfatide molecules bound to each MD-2 pocket, with at most three molecules bound per pocket. The heterogeneity in the number of C16-sulfatide molecules bound may also explain the very small downshift of monomeric mTLR4–MD-2–C16-sulfatide relative to monomeric apo mTLR4–MD-2 in the native PAGE (Fig. 4*A*, lane 4 vs. lane 1). After refinement, the overall configurations of the six lipid chains inside the mMD-2 hydrophobic pocket were well-resolved (Fig. 4*D*). However, the other parts of the C16-sulfatide molecules, including the hydroxyl and amide groups of the ceramide moiety, the galactose moiety, and the sulfate group, all of which were outside the mMD-2 pocket, had poorly defined electron densities, likely due to the flexibilities of these groups in the structure, and we were unable to determine their conformations (Fig. 4*D*). Partial densities from the hydroxyl and amide groups of the ceramide moiety from one of the three C16-sulfatide molecules allowed us to decide which two lipid chains were connected in each of the three C16-sulfatide molecules. Overall, the dimeric mTLR4–MD-2–C16-sulfatide complex was highly similar in structure to other ligand-induced active TLR4–MD-2 complexes.

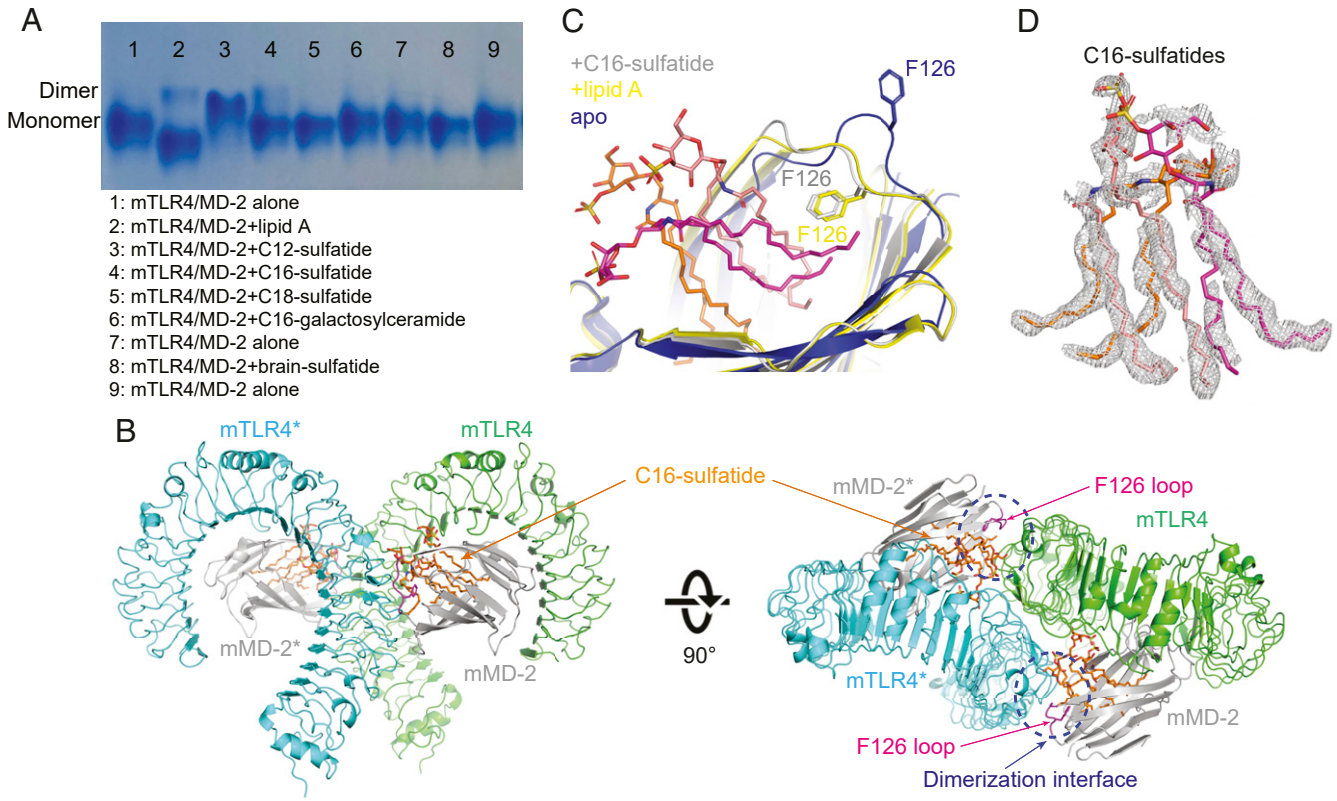

Fig. 4. C16-sulfatide binds directly to mTLR4–MD-2 and induces an active dimer structure. (*A*) Native PAGE analysis of mTLR4–MD-2 alone (50 μM) and in the presence of lipid A (300 μM), sulfatides (1 mM), or C16-galactosylceramide (1 mM). A superimposed densitometric profile of the gel lanes is included in *SI Appendix*, Fig. S4 to better illustrate the small downward shift of the monomer band caused by C16-, C18-, or brain-derived sulfatide binding compared with the monomer band of apo mTLR4–MD-2. (*B*) Orthogonal views of the overall crystal structure of mTLR4–MD-2–C16-sulfatide. (*C*) Superposition of mMD-2 from the crystal structures of mTLR4–MD-2–C16-sulfatide, mTLR4–MD-2–lipid A (PDB ID code 5IJD), and apo mTLR4–MD-2 (PDB ID code 5IJB) showing similar local conformational changes in the Phe126 loop area for both agonist-bound structures. The three bound C16-sulfatide molecules are shown as sticks. (*D*) 2Fo − Fc composite omit electron density map generated using PHENIX (contoured at 1.0σ) of the three molecules of C16-sulfatide in the crystal structure, shown as orange, pink, and magenta sticks.

The C16-Sulfatide Binding Site in mTLR4–MD-2. To define the overall conformations of the three C16-sulfatide molecules, we performed molecular dynamics (MD) simulation studies using the crystal structure of the mTLR4–MD-2–C16-sulfatide complex. The overall MM-PBSA-WSAS (molecular mechanics–Poisson–Boltzmann surface area–weighted solvent-accessible surface area) binding free energy (35, 37) calculated for the dimeric mTLR4–MD-2 in complex with six C16-sulfatides (three C16-sulfatides in each monomeric mTLR4–MD-2) was −147.7 kcal/mol, which suggested potent interactions between the three C16-sulfatides and each mTLR4–MD-2. The representative MD structure had a main-chain rmsd of 0.89 Å to the average MD structure obtained by averaging 25,000 MD snapshots, and an rmsd of 1.64 Å to the crystal structure (*SI Appendix*, Fig. S6*B*).

The three C16-sulfatide molecules in the representative MD structure, designated SUL-A, SUL-B, and SUL-C, adopted different conformations and interacted with different regions of mTLR4–MD-2 and mTLR4* (Fig. 5 *A* and *B*). The sphingosine chain (S1) of SUL-A and the four lipid chains of SUL-B and SUL-C were buried and formed hydrophobic contacts with many residues of mMD-2 (Fig. 5*B* and *SI Appendix*, Table S2). The SUL-A FA chain (S2) was located at the interface between mMD-2 and mTLR4* and interacted with hydrophobic residues of mTLR4*, such as Phe438, to facilitate dimerization of mTLR4–MD-2. At the dimerization interface, four hydrogen bonds were observed between C16-sulfatides and mTLR4* (Fig. 5*B* and Table 1), including two between the sulfate group of SUL-B and the backbone amine and carbonyl groups of Ser386, one between the carbonyl group of the SUL-B S2 chain and the side chain of Ser413, and one between the oxygen atom of the pyranose ring of the galactose moiety of SUL-A and the side chain of Arg434. In addition, two hydrogen bonds formed between the backbone amine and carbonyl groups of mMD-2 Leu125 and the side chain of mTLR4* Asn415 (Fig. 5*B*); these two hydrogen bonds are also observed in the crystal structures of all active TLR4–MD-2 dimers (8, 32, 34). Several hydrogen bonds were also observed between the C16-sulfatides and mTLR4 and mMD-2 (Fig. 5*B* and Table 1). In particular, mMD-2 Arg90 formed two hydrogen bonds with the carbonyl group of the SUL-A S2 chain and was located at the dimerization interface.

We performed site-directed mutagenesis of mTLR4 and mMD-2 to confirm the key interactions involved in receptor dimerization and the interactions between C16-sulfatides and the receptor complex predicted by MD simulation studies. Nineteen residues with binding energy equal to or better than −4.0 kcal/mol were mutated to alanine (*SI Appendix*, Fig. S7 *A* and *B* and Table S2). mTLR4* Asn415 formed hydrogen-bonding interactions with mMD-2 Leu125 at the dimerization interface and these two residues were also mutated to alanine. Mutant proteins with expression levels similar to the wild-type protein (9 of 10 mTLR4 mutants and 10 of 11 mMD-2 mutants) were tested for their ability to activate NF-κB–dependent luciferase reporter activity in HEK293T cells stimulated with C16-sulfatide, C12-sulfatide, or lipid A (Fig. 5 *C*–*E*). The responses of cells expressing mutant proteins were compared to identify residues involved in protein–protein or protein–ligand interactions induced by each ligand. C12-sulfatide was

compared with C16-sulfatide to reveal the effects of the FA chain length on interactions with mTLR4–MD-2.

Interactions at the dimerization interface and interactions between ligands and mTLR4–mMD-2. Mutating the residues located at the dimerization interface and in the mMD-2 Phe126 loop region resulted in similar effects on NF-κB–dependent luciferase reporter activation in response to C16- and C12-sulfatides and lipid A (Fig. 5 *C*–*E*). In particular, mutations of mMD-2 Arg90 and mTLR4* Asn415 and Phe438, and all mutations in the mMD-2 Phe126 loop region, severely reduced the responsiveness to all stimuli. The mTLR4* Arg434Ala mutation reduced the responsiveness to C16-sulfatide, C12-sulfatide, and lipid A by about 80, 45, and 55%, respectively, suggesting a nonessential supporting function for Arg434 in dimerization and activation of mTLR4–MD-2 induced by all three stimuli. Mutating most residues from mTLR4 and mMD-2 that formed hydrogen bonds with the C16-sulfatides,

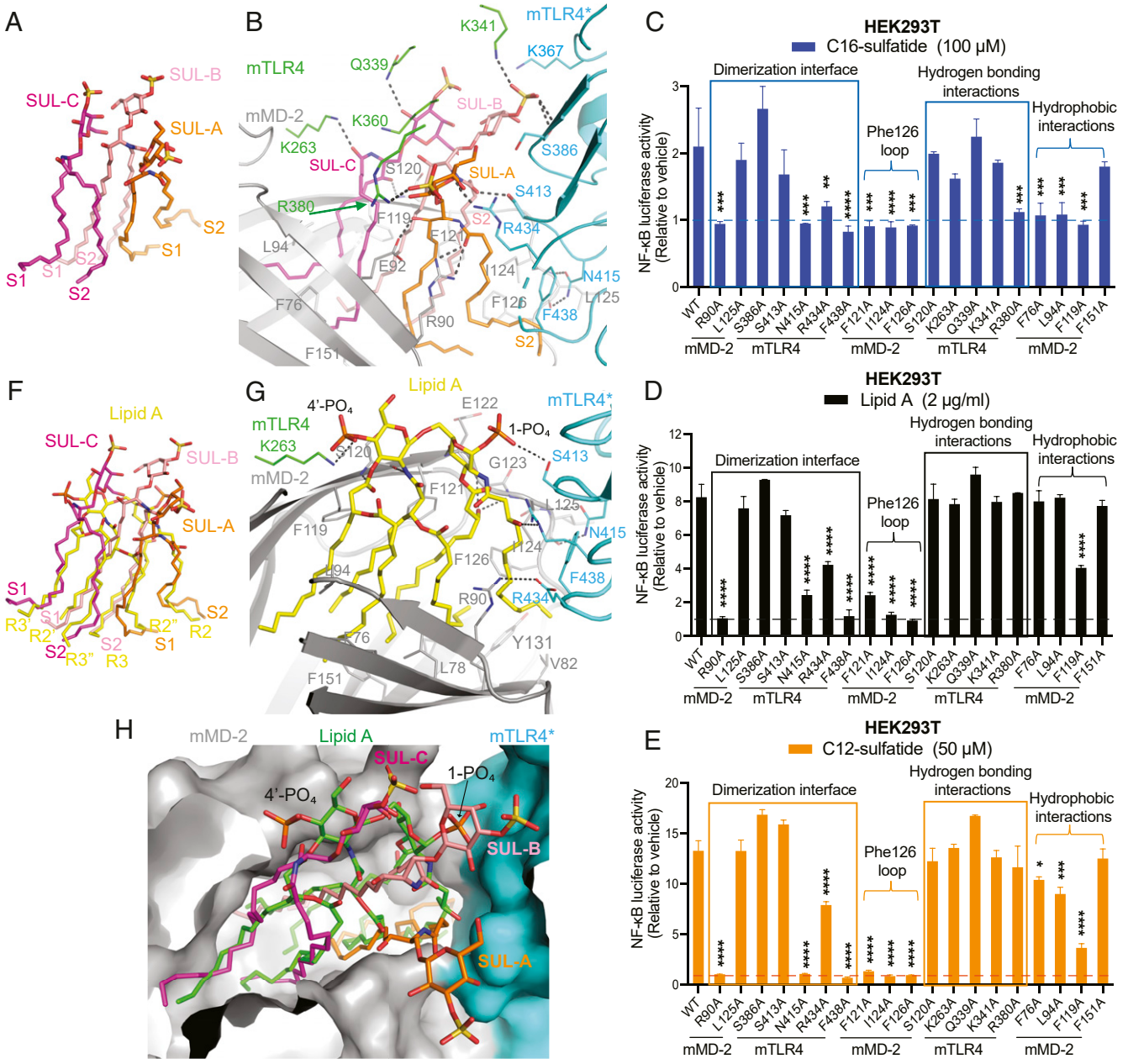

Fig. 5. Similarities and differences in binding of C16-sulfatide and lipid A to mTLR4–MD-2. The structures of mTLR4–MD-2–C16-sulfatide shown here are from molecular dynamics simulation. (*A*) Stick representation of the three C16-sulfatide molecules: SUL-A, SUL-B, and SUL-C. (*B*) Enlarged view of the dimerization interface showing interactions of SUL-A, SUL-B, and SUL-C with mTLR4, mMD-2, and mTLR4*. (*C*–*E*) NF-κB–dependent luciferase activity in HEK293T cells transiently expressing mTLR4 and mMD-2 bearing the indicated mutations and stimulated with C16-sulfatide (100 μM) (*C*), lipid A (2 μg/mL) (*D*), or C12-sulfatide (50 μM) (*E*) for 5 h; $n = 2$. WT indicates cells expressing WT mTLR4 and mMD-2. Data are representative of at least two independent experiments. $^{*}P < 0.05$, $^{**}P < 0.01$, $^{***}P < 0.001$, $^{****}P < 0.0001$ (one-way ANOVA followed by Dunnett's posttest for comparison with the WT condition). Data (mean ± SEM) were normalized to luciferase activity measured in cells expressing the same mutations and stimulated with vehicle (water). A dashed line at the *y*-axis value of 1 is shown to indicate reporter activation by vehicle. (*F*) Superposition of mMD-2 (not shown) from structures of mTLR4–MD-2–C16-sulfatide and mTLR4–MD-2–lipid A showing the overlapping of C16-sulfatides and lipid A. (*G*) Enlarged view of the dimerization interface showing interactions of lipid A with mTLR4, mMD-2, and mTLR4* (PDB ID code 5IJD). (*H*) Surface presentation of the mMD-2 hydrophobic pocket and the dimerization interface between mMD-2 and mTLR4* showing the differences in binding of C16-sulfatides and lipid A to these areas.

Table 1. Summary of the hydrogen bonds between C16-sulfatide and mTLR4, mMD-2, and mTLR4* from the MD representative structure

C16-sulfatide molecule-chain	C16-sulfatide group	Protein chain	Residue	Residue group
A	Galactose moiety	mTLR4*	Arg434	Side chain
B-S2 chain	Carbonyl	mTLR4*	Ser413	Side chain
B	Sulfate	mTLR4*	Ser386	Amide NH
B	Sulfate	mTLR4*	Ser386	Amide carbonyl
A	Sulfate	mTLR4	Arg380	Side chain
B	Sulfate	mTLR4	Lys341	Side chain
C-S2 chain	Carbonyl	mTLR4	Lys263	Side chain
C	Galactose moiety	mTLR4	Gln339	Side chain
A-S2 chain	Carbonyl	mMD-2	Arg90	Side chain
A-S1 chain	Hydroxyl	mMD-2	Glu92	Side chain
C-S1 chain	Hydroxyl	mMD-2	Ser120	Amide NH

The key hydrogen-bonding interactions were confirmed with mutagenesis experiments.

including Lys263, Gln339, Lys341, and mMD-2 Ser120, did not significantly affect the activity of any stimulus (Fig. 5 *C*–*E*). However, mutation of Arg380, which interacted with the sulfate group of SUL-A (Fig. 5*B*), dramatically decreased the activity of C16-sulfatide (Fig. 5*C*) but not C12-sulfatide or lipid A, confirming the conformation of this sulfate group determined by MD simulation.

Interactions between ligands and the mMD-2 hydrophobic pocket. Mutations of the residues located inside the mMD-2 hydrophobic pocket showed different effects on NF-κB–dependent luciferase reporter activation in response to C16- and C12-sulfatides and lipid A (Fig. 5 *C*–*E*). In particular, mutations of Phe76, Leu94, and Phe119 abolished the responsiveness to C16-sulfatide (Fig. 5*C*), and reduced the responsiveness to C12-sulfatide by about 23, 35, and 82% (Fig. 5*D*), respectively, whereas only Phe119Ala reduced the responsiveness to lipid A by about 58% (Fig. 5*E*). These data showed that the activity of C12-sulfatide was less affected by these mutations than the activity of C16-sulfatide, likely reflecting that C12-sulfatide bound to the mMD-2 hydrophobic pocket with higher affinity than C16-sulfatide. This hypothesis is consistent with the higher potency of C12-sulfatide in inducing TNFα in mouse macrophages (Fig. 1*B*) and in inducing mTLR4–MD-2 dimerization in vitro (Fig. 4*A*).

Overall, of 17 tested residues with binding energy equal to or better than −4.0 kcal/mol, 10 resulted in diminished C16-sulfatide–induced NF-κB reporter activity when mutated to alanine. These data support the MD simulation structure of the mTLR4–MD-2–C16-sulfatide complex. As expected, fewer of the tested mutations altered reporter activity induced by lipid A (7/17) or C12-sulfatide (9/17) compared with the number that altered activity induced by C16-sulfatide; this is likely because identified hotspot residues (*SI Appendix*, Table S2) were specific to the C16-sulfatide–bound receptor complex.

Short FA Chain Sulfatides Activate mTLR4–MD-2 through a Slightly Different Structural Mechanism from That of Lipid A. Comparison of the bound C16-sulfatides and lipid A revealed that the lipid chains of the three C16-sulfatides and lipid A overlapped well (Fig. 5*F*). S1 chains of SUL-A, SUL-B, and SUL-C overlapped with the R2′′, R2′, and R3′ chains of lipid A, respectively. S2 chains of SUL-A, SUL-B, and SUL-C overlapped with the R2, R3, and R3′′ chains of lipid A, respectively. On the other hand, the galactose moiety and sulfate groups adopted different conformations and made contacts with mTLR4–MD-2 distinct from those of the phosphoglucosamine groups of lipid A (Fig. 5 *B*, *F*, and *G*).

The lipid chains of C16-sulfatide (one 18-carbon chain and one 16-carbon chain) are longer than those of lipid A (five 14-carbon chains and one 12-carbon chain). As a result, the galactose moieties and sulfate groups of C16-sulfatides protruded out of the mMD-2 hydrophobic pocket farther than the phosphoglucosamine groups of lipid A (*SI Appendix*, Fig. S8*A*). The sulfate group of SUL-B formed hydrogen bonds with the backbone atoms of mTLR4* Ser386; these bonds were not present in the mTLR4–MD-2–lipid A structure (Fig. 5 *B* and *G*). At the entrance of the MD-2 hydrophobic pocket next to the Phe126 loop, five hydrogen bonds were observed between mMD-2 residues, including Ser120, Glu122, and Gly123, and the glucosamine moiety, and the hydroxyl, amine, and carbonyl groups from the lipid chains of lipid A. These interactions pulled the phosphoglucosamine groups of lipid A toward one side of the MD-2 pocket and likely stabilized the conformation of these groups (*SI Appendix*, Fig. S8*B*). However, only one hydrogen bond in this region was observed between the backbone atoms of mMD-2 Ser120 and the hydroxyl group of the S1 chain of SUL-C (*SI Appendix*, Fig. S8*C*). Unlike lipid A, the galactose moiety and sulfate groups of SUL-A, SUL-B, and SUL-C occupied most of the space above the MD-2 pocket (Fig. 5*H*). Several other hydrogen bonds were observed between these groups, mTLR4, and mMD-2 and were not present in the mTLR4–MD-2–lipid A structure (Fig. 5 *B* and *G* and Table 1). The sulfate group of SUL-A made an additional contact, not present in the mTLR4–MD-2–lipid A structure, with the side chain of mTLR4 Arg380 (Fig. 5 *B*, *G*, and *H*). This interaction was key for the activity of C16-sulfatide but not for lipid A or C12-sulfatide.

The dimerization interface contains similar interactions in the mTLR4–MD-2–C16-sulfatide and mTLR4–MD-2–lipid A structures. These include hydrophobic interactions between mTLR4* and the R2 chain of lipid A or S2 chain of SUL-A, and hydrogen bonding between mTLR4* and the R2-OH and 1-PO_4 of lipid A or S2-carbonyl and sulfate groups of SUL-B (Fig. 5 *B* and *G*). Overall, three molecules of C16-sulfatide bound together to the mMD-2 hydrophobic pocket and partially mimicked the interactions and activation mechanism of lipid A to induce an active 2:2 mTLR4–MD-2 dimer conformation very similar to that induced by other agonists, such as lipid A and neoseptin-3.

Residues Involved in Species Specificity for Sulfatides. Of the residues that were important for the activity of C12- and C16-sulfatides (Fig. 5 *C* and *E*) and the hotspot residues that showed ligand binding energy close to −4 kcal/mol (*SI Appendix*, Table S2), Arg434 and Lys367 are not conserved between mouse and human TLR4. These two residues are located at the dimerization interface; Lys367 is located near the sulfate group of SUL-B, while Arg434 interacts with the galactose moiety of SUL-A (Fig. 5*B*). To test whether these two residues play important roles in the species-specific agonistic activity of C12- and C16-sulfatides, mouse TLR4 Arg434 and Lys367 were mutated to their human counterparts, Gln436 and Glu369, respectively, and the human residues were mutated to their respective mouse residues (*SI Appendix*, Fig. S7 *C* and *D*). We tested the responsiveness of these mutants to C16-sulfatide,

lipid A, and C12-sulfatide in HEK293T cells that stably expressed an NF-κB–driven luciferase reporter.

mTLR4 Lys367Glu and Arg434Gln mutations significantly reduced the NF-κB reporter activity stimulated by C12- and C16-sulfatides, and slightly decreased the activity induced by lipid A (Fig. 6 *A* and *B*). Double mutation of these two residues further reduced the agonistic activities of the sulfatides (Fig. 6 *A* and *B*). Single or double mutations of these two residues in human TLR4, Glu369Lys, Gln436Arg, or Glu369Lys/Gln436Arg, slightly enhanced responsiveness to LPS but did not confer responsiveness to C16-sulfatide. Strikingly, Glu369Lys and Gln436Arg mutations conferred responsiveness to C12-sulfatide (50 to 75% of the wild-type response induced by LPS), whereas C12-sulfatide had shown only weak agonistic activity when applied to human cells endogenously expressing wild-type human (h) TLR4 (5 to 10% of the response induced by lipid A; Fig. 1*C*). Moreover, hTLR4 carrying the double mutation Glu369Lys/Gln436Arg became as responsive to C12-sulfatide as to LPS. These results suggest that Lys367 and Arg434 are important for the species specificity of C12-sulfatide, possibly because they enhance the electrostatic potential at the dimerization interface and facilitate the interaction between C12-sulfatide and TLR4* for dimerization and activation.

Discussion

Our structural data revealed that three molecules of C16-sulfatide bound to the mMD-2 hydrophobic pocket in each mTLR4–MD-2 heterodimer, resulting in dimerization and activation of the heterodimer via interactions and conformational changes partially mimicking those induced by lipid A. Compared with lipid A, the C16-sulfatides protrude farther out of the MD-2 pocket, probably due to their longer lipid chains (18/16 vs. 14/12). No interactions were observed between those groups of the three C16-sulfatides positioned outside the MD-2 pocket. This lack of interaction and costabilization could contribute to their flexibilities, the heterogeneity in the number of C16-sulfatides simultaneously bound to each MD-2, and the heterogeneity in the quality of the electron densities of each C16-sulfatide observed in the crystal structure. The reduced potency of C16-sulfatides compared with lipid A in activating mouse TLR4–MD-2 may be a result of a lower binding affinity, the necessity for three molecules (rather than one) to bind simultaneously, and greater flexibility of C16-sulfatide molecules relative to lipid A in the MD-2–binding pocket. Our biological, in vitro biochemical, and structural data suggest that other lipids containing up to six acyl chains of a certain length and a negatively charged group may be capable of binding to TLR4–MD-2 as agonists or antagonists. A combination of several molecules with one to three acyl chains or one molecule with four to six acyl chains may be able to do so. Globotetraosylceramide (Gb4Cer), a glycosphingolipid containing a 4-mer oligosaccharide but no sulfate, binds mouse MD-2 and inhibits LPS-stimulated activity (38). Furthermore, while Gb3Cer and Gb4Cer alone have no effect on TLR4 signaling, a recent report suggested that these glycosphingolipids bind TLR4 in the presence of LPS and enhance LPS activity (39).

In contrast to its agonist activity toward mouse TLR4–MD-2, C16-sulfatide displayed antagonist activity toward the human receptor even at low concentrations, suggesting that one to three molecules of C16-sulfatide may also bind to human TLR4–MD-2. We have determined, in part, the reason for the species difference at the atomic level. Human TLR4 with the single mutations Glu369Lys or Gln436Arg became responsive to C12-sulfatide and the double mutant was activated by C12-sulfatide and LPS to the same extent. This behavior similarly applies to lipid IVa (40), which is also an agonist for mouse TLR4–MD-2 and an antagonist for human TLR4–MD-2. Our results confirm the importance of electrostatic potentials at the dimerization interface of TLR4–MD-2 for determining activating versus antagonistic effects of ligands by contributing to the proper positioning of LPS and related ligands such as lipid IVa (34).

The fact that sulfatides with specific chain lengths are active, and the fact that a major difference between the responses of human and mouse cells is observed for individual ligands, may explain some of the conflicting published reports on sulfatide effects introduced earlier. The significance of the central finding that specific short FA chain sulfatides bind and elicit activating conformational changes in mouse TLR4–MD-2 complexes must

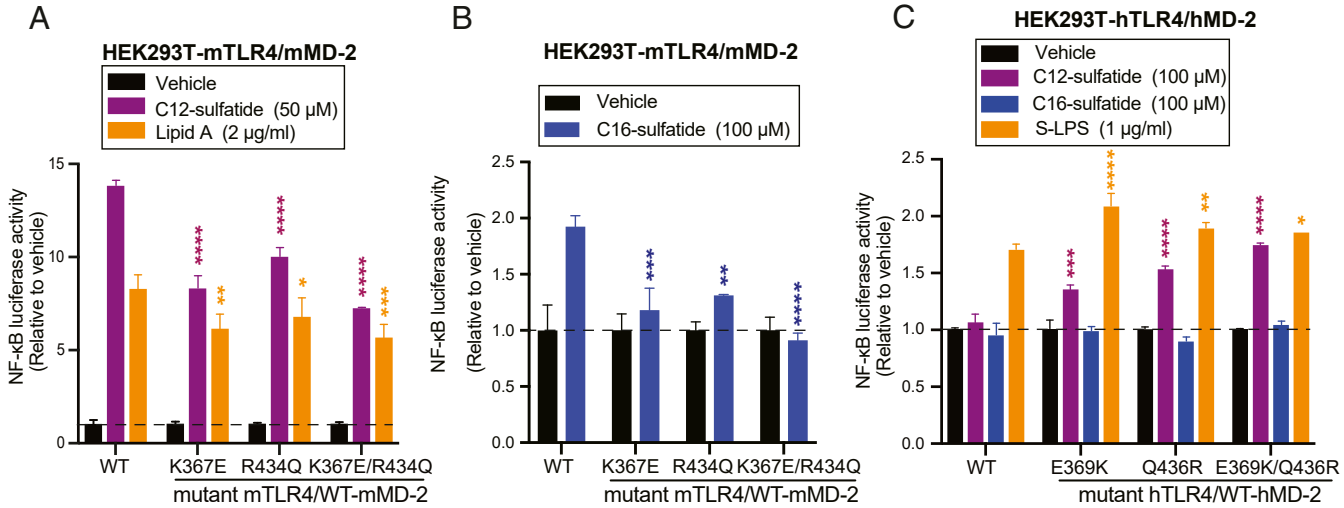

Fig. 6. Residues involved in species specificity for short FA chain sulfatides. (*A* and *B*) NF-κB–dependent luciferase activity in HEK293T cells transiently expressing mTLR4 and mMD-2 bearing the indicated mutations and stimulated with C12-sulfatide (50 μM) or lipid A (2 μg/mL) (*A*), or C16-sulfatide (100 μM) (*B*) for 5 h; $n = 2$. (*C*) NF-κB–dependent luciferase activity in HEK293T cells transiently expressing hTLR4 and hMD-2 bearing the indicated mutations and stimulated with C12-sulfatide (100 μM), C16-sulfatide (100 μM), or smooth LPS (1 μg/mL) for 5 h; $n = 2$. WT indicates cells expressing WT mTLR4 and mMD-2 (*A* and *B*) or cells expressing WT hTLR4 and hMD-2 (*C*). Data (mean ± SEM) are representative of at least two independent experiments. $^*P < 0.05$, $^{**}P < 0.01$, $^{***}P < 0.001$, $^{****}P < 0.0001$ (two-way ANOVA followed by Dunnett's posttest for comparison with the WT condition treated with the same ligand). Data were normalized to luciferase activity measured in cells expressing the same mutations and stimulated with vehicle (water) control. There is no reporter activation when the *y*-axis value equals 1 (shown with a dashed line).

be assessed in the context of the relative abundance and bioavailability of the bioactive species, both under normal and pathologic conditions. We demonstrated by dynamic light scattering analysis that C12-, C16-, C18-, and brain-derived sulfatides all formed vesicles in solution at a concentration of 5 μM (*SI Appendix*, Fig. S1). Therefore, at the concentrations at which C12-sulfatide and C16-sulfatide showed cellular activity but C18-sulfatide and brain-derived sulfatides did not, all of these sulfatide species were predominantly vesicular. These findings argue against the idea that reduced aggregation of short FA chain sulfatides resulting in increased free sulfatide molecules underlies the greater potency of short FA chain sulfatides compared with longer FA chain sulfatides. We hypothesize that longer FA chains have more difficulty burying their hydrocarbon chains into the MD-2 hydrophobic pocket and protrude farther out of the MD-2 hydrophobic pocket; the exposed hydrophobicity may result in poorer binding to MD-2 compared with the binding of short FA chain species. Thus, the binding of three short FA chain sulfatides would be favored compared with the binding of three long FA chain sulfatide molecules. We do not yet have a clear picture of how sulfatides access the receptor; other molecules in the culture medium or in vivo, such as serum lipoproteins, other sulfatides, or lipids, may alter the physical state of sulfatides (e.g., from vesicular to free molecules), or lipid-binding proteins may facilitate binding of sulfatides to TLR4–MD-2 similar to LBP and CD14 facilitating the binding of LPS to the receptor (26, 27).

The relative abundance of sulfatide species with particular acyl chain lengths varies within different cell types in different tissues. Sulfatide species abundance may be directly impacted by ceramide synthases (CerSs) (41), multispanning membrane proteins that catalyze the transfer of FAs to dihydrosphingosine. Six CerSs exist in mammals (42), each with a characteristic preference for FAs with a restricted range of acyl chain length. For example, CerS5 and CerS6 preferentially transfer short acyl chain substrates (C14 and C16) to dihydrosphingosine (42, 43). The lengths of FAs themselves are specified by soluble cytoplasmic FA synthases or endoplasmic reticulum membrane-anchored very long chain FA synthases (44). The expression and activity of these enzymes may ultimately influence the quantities and proportions of sulfatides in specific cell types. Renal cells, cells of the gastrointestinal tract, pancreatic islet cells, and particularly brain cells are sulfatide-rich (9) but different sulfatide chain lengths predominate in different cells within these tissues (13). For example, the ratio between C24- and C16-sulfatides is roughly 10, 1, and 0.1 in the brain, pancreas, and blood, respectively (18). C12:0 sulfatide, while very active in our studies, has not been reported to exist at detectable concentrations in mammalian tissues. C14:0 sulfatide is of low abundance in human cortical brain cells (where C18:0 and C24:1 are most abundant) (33) but is undetectable in kidney, where C16-, C22-, and C24-acyl chains are most abundant (13, 45).

Do biologically relevant concentrations of active sulfatide species become bioavailable under pathologic conditions and contribute to pathology? Sulfatides are particularly abundant glycolipids in lipid bilayers of the myelin sheaths formed by oligodendrocytes (46, 47), and in neurons and astrocytes (48, 49). A possible role in central nervous system (CNS) pathology, mediated by TLR4–MD-2 interactions, is therefore to be suspected. It has previously been observed that during the paralytic phase of EAE in mice, the amount of brain C14:0 sulfatide rises more than 10-fold, while the amount of C16:0 sulfatide drops considerably (50). More recently it was noted that humans with MS produce sulfatide-specific autoantibodies, as do mice with EAE (12). Moreover, immunization of SJL/J mice with myelin-derived peptides plus sulfatide caused a more severe course of EAE than immunization against myelin-derived peptides alone, and administration of sulfatide-specific antibody exacerbated EAE (12). These data might be interpreted in light of the fact that sulfatides of a given range of FA chain length act, in mice, as TLR4–MD-2 agonists.

Short FA chain sulfatides present endogenously would exert TLR4-mediated adjuvant effects in mice, causing a type 1 T-independent antibody response directed against themselves, as well as T-dependent augmentation of antibody responses directed against immunodominant peptides from myelin. Antibodies reactive with sulfatides or myelin peptides might cause complement-dependent CNS pathology. Sulfatide-binding antibodies might actually increase endogenous sulfatide bioavailability by conferring solubility to a normally hydrophobic molecule, leading to increased TLR4–MD-2–mediated inflammation, and the further release of endogenous sulfatides from inflamed, damaged tissue, creating a feedforward cycle. It is possible that similar sulfatide-mediated immune responses may be related to immunopathogenesis in other tissues rich in short FA chain sulfatides, notably the kidneys and β-cells of pancreatic islets. While our data suggest that reactions of this type may not operate in humans, at least 50 different native subspecies of ceramide, and hence sulfatide, exist in mammals, varying by FA chain length, double-bond saturation and hydroxylation, and sphingosine base saturation (9, 51, 52). Thus, we cannot exclude the possibility that particular sulfatide subspecies might be found to activate human TLR4–MD-2. We also speculate that other physiological lipids may activate human TLR4–MD-2, leading to autoinflammatory disease via these mechanisms. Cardiolipin is one such candidate lipid, which is a target of antibodies in antiphospholipid syndrome and other inflammatory diseases. Saturated cardiolipin was recently reported to activate TLR4–MD-2 in primary human monocytes and mouse macrophages (53). The role of TLR4 might be tested using TLR4-deficient mice in an induced model of antiphospholipid syndrome caused by anticardiolipin administration.

Materials and Methods

Sources of mice and reagents are provided in *SI Appendix, Materials and Methods*.

Isolation of Bone Marrow–Derived Macrophages and Peritoneal Macrophages. Female wild-type (WT) C57BL/6, TLR4-knockout, TRIF-knockout, and MyD88-knockout mice (6 to 8 wk old) were killed and the femoral and tibial marrow was flushed with culture medium supplemented with 10% fetal bovine serum (FBS) using a 26-gauge needle. Following centrifugation, the cells were resuspended in culture medium supplemented with 20% FBS and 30% L929 cell conditioned medium (macrophage colony-stimulating factor source), seeded in Petri dishes at a density of 5.6×10^4 cells per square centimeter, and incubated at 37 °C in a humidified incubator with 5% CO_2. After 2 d, fresh medium was added. On day 7, the culture medium was replaced and the adherent cells (differentiated BMDMs, ~98% homogeneous by appearance) were transferred to storage in liquid N_2 until used.

Peritoneal macrophages from WT C57BL/6J, $Tlr4^{lps3/lps3}$, $Tlr2^{-/-}$, and $Cd14^{hdl/hdl}$ mice were isolated 4 d after intraperitoneal injection of 2 mL BBL thioglycollate medium, brewer modified (4% [weight/volume]; BD Biosciences) by peritoneal lavage with 5 mL of phosphate-buffered saline (PBS). The peritoneal macrophages were cultured in Dulbecco's modified Eagle's medium (DMEM) containing 2% FBS and 1% penicillin and streptomycin (Life Technologies).

Cell Culture. Mouse RAW264.7 macrophage cells, human THP-1 monocytes, and SW620 cells (ATCC) were grown to 80 to 90% confluence in DMEM supplemented with 8 mM L-glutamine, 100 U/mL penicillin, 100 μg/mL streptomycin, and 1,250 U/mL nystatin, with 10% heat-inactivated FBS. THP-1 monocytes were grown in suspension up to 8×10^5 cells per milliliter in RPMI medium 1640 supplemented with 2 mM L-glutamine, 10 mM Hepes, 50 μM 2-mercaptoethanol, 100 U/mL penicillin, 100 μg/mL streptomycin, and 1,250 U/mL nystatin, with 10% heat-inactivated FBS. SW620 colon epithelial cancer cells were grown to 70 to 80% confluence in culture medium identical to the THP-1 culture medium except 2-mercaptoethanol was omitted. Cells were incubated at 37 °C in a humidified incubator with 5% CO_2.

TNF Release Assay. RAW264.7 macrophages were maintained for 24 h prior to the experiment in 96-well plates, at 1.5×10^5 cells per well, in culture medium supplemented with 10% FBS, up to a confluence of 90%. The culture medium

was replaced with fresh culture medium containing 5% heat-inactivated FBS 2 h before treatment. The cells were treated as indicated at 37 °C for 4 or 24 h.

THP-1 monocytes were differentiated in the presence of 100 nM PMA for 24 h. Cells were washed with PBS and cultured in fresh RPMI medium for 24 h before use in stimulation experiments.

Mouse peritoneal macrophages or THP-1 cells were plated in 96-well plates at a density of 1×10^5 or 0.5×10^5 cells per well, respectively. Cells were stimulated with sulfatides, controls, lipid A, or LPS for 4 h. Inhibition experiments were done with pretreatment of the cells with sulfatides, C16-galactosylceramide, or vehicle control for 1 h before stimulation with lipid A, or for 5 min before stimulation with LPS. Mouse or human TNF in the culture media was measured using an enzyme-linked immunosorbent assay kit according to the manufacturer's instructions (Invitrogen or R&D Systems).

Luciferase Assays for NF-κB Activation. HEK293T cells stably expressing an NF-κB–driven luciferase reporter were cultured in DMEM supplemented with 10% FBS and plated in 96-well plates at 0.7×10^5 cells per well 18 h before transfection. Plasmids encoding WT or mutant TLR4 and MD-2 from mice or humans were cotransfected into cells in each well using Lipofectamine 2000 (Life Technologies). Twenty-four hours after transfection, cells were stimulated with 50 μM C12-sulfatide, 100 μM C16-sulfatide, or 2 μg/mL lipid A for 5 h. Cells were lysed and luciferase activity in each well was measured using the Steady-Glo Luciferase Assay System (Promega). Data were expressed as a ratio of NF-κB–dependent luciferase activity stimulated with lipids divided by the luciferase activity measured in cells expressing the same mutations and stimulated with vehicle (water).

RAW264.7 macrophages were grown for 24 h in 24-well plates, at 1.5×10^5 cells per well, in culture medium supplemented with 10% FBS. The cells were then transfected for 24 h with 0.2 μg of NF-κB reporter plasmid and 0.07 μg of herpes simplex virus TK-renilla luciferase. The plasmids were initially incubated with TransIT2020 transfection reagent (Mirus Bio) in OptiMEM for 20 to 30 min at room temperature. Following transfection, the cells were washed and stimulated as indicated at 37 °C for 4 h, after which luciferase activity in cell extracts was determined following the manufacturer's instructions (Promega). Data were expressed as a ratio of NF-κB–driven luciferase activity divided by the renilla luciferase activity, and relative to control untreated cells.

SW620 epithelial cells were grown for 24 h in 24-well plates, at 2×10^5 cells per well, in SW620 culture medium supplemented with 10% FBS. The cells were then transfected for 24 h with 0.2 μg of mouse TLR4 and/or 0.2 μg of mouse MD-2 (or the pcDNA vector), 0.1 μg of NF-κB reporter plasmid, and 0.05 μg of herpes simplex virus TK-renilla luciferase, using Lipofectamine 2000. Cells were washed and stimulated as indicated at 37 °C for 4 h, after which luciferase activity in cell extracts was determined following the manufacturer's instructions (Promega). Data were expressed as a ratio of NF-κB–driven luciferase activity divided by the renilla luciferase activity, and relative to control untreated cells.

Immunoblot Analysis. Whole-cell lysates were prepared using RIPA buffer as previously described (54). Protein concentration was determined by a modification of the Bradford procedure (55). Bovine serum albumin served as a standard. Two-color imaging and quantitative analysis of immunoblots were performed using infrared dye–labeled secondary antibodies and blocking buffer and the Odyssey Infrared Imaging System (Li-Cor Biosciences), according to the manufacturer's instructions.

Sulfatide Vesicle Preparation. C12-sulfatide and C16-galactosylceramide were dissolved in a mixture of chloroform, methanol, and water with a volume (vol) ratio of 4:1:0.1. Porcine brain sulfatide was dissolved in a 2:1:0.1 (vol:vol:vol) solution of chloroform:methanol:water. C16- and C18-sulfatides were dissolved in 2:1 (vol:vol) and 5:1 (vol:vol) solutions of chloroform:methanol, respectively. These lipids were dried in glass vials with nitrogen gas and further dried under vacuum overnight. The lipid films were resuspended in endotoxin-free water with cycles of freeze, thaw, and sonication in a water bath for 5 min. In some experiments, additional tip sonication was applied for two rounds of 10 s. The C16-sulfatide used in the experiment shown in *SI Appendix*, Fig. S2*C* was dissolved in a 4:1 (vol:vol) solution of chloroform:methanol, dried in glass vials with nitrogen gas and then under vacuum overnight, and dissolved in dimethyl sulfoxide (DMSO).

Protein Expression, Purification, and Crystallization. The recombinant mouse TLR4–MD-2 complex was coexpressed in High Five insect cells and purified as described (8). Fully purified mTLR4–MD-2 (8.8 mg/mL) was incubated with 500 μM C16-sulfatide vesicles at 37 °C for 4 h. The mTLR4–MD-2 and C16-sulfatide mixture was buffer-exchanged to a buffer containing 25 mM Hepes (pH 8.0) and 75 mM NaCl by concentration and dilution three times using a 50-kDa concentrator. The complex was then concentrated to 20 mg/mL for crystallization.

The mTLR4–MD-2–C16-sulfatide crystals were grown with a hanging-drop vapor-diffusion method by mixing 1 μL of protein and 1 μL of reservoir buffer containing 0.1 M Tris (pH 8.0), 0.8 M sodium formate, 8% polyethylene glycol (PEG) 8000, and 8% PEG 1000. The mTLR4–MD-2–C16-sulfatide crystals were flash-frozen in liquid nitrogen in a cryoprotection buffer containing 0.1 M Tris (pH 8.0), 0.8 M sodium formate, 50 mM NaCl, 9% PEG 8000, and 40% PEG 1000.

Data Collection and Structure Determination. Diffraction data were collected at beamline 19-ID (Structural Biology Center Collaborative Access Team) at the Advanced Photon Source (Argonne National Laboratory). The data were indexed, integrated, and scaled using the HKL-3000 package (56). The phase was obtained from the molecular replacement method using the program Phaser (57). The published mouse TLR4–MD-2–neoseptin-3 structure (PDB ID code 5IJC) was used as a search model. The electron densities for the six lipid chains of C16-sulfatide inside the MD-2 hydrophobic pocket were clear enough to allow us to build the atomic models of these lipid chains into the density map. The electron densities for the galactose moiety and sulfate group were very poor, probably due to the flexibility of these groups. The manual model building was performed with the program Coot (58) and the crystallographic refinement was performed using the program PHENIX (59). Positional and isotropic atomic displacement parameter (ADP) as well as translation–libration–screw-rotation ADP refinement was performed during refinement with a random small percentage of all data set aside for an R_{free} calculation. Data collection and structure refinement statistics are summarized in *SI Appendix*, Table S1.

Molecular Dynamics Simulation. Molecular dynamics simulations were performed for the dimeric TLR4–MD-2 in complex with C16-sulfatide. The neutralized MD simulation systems consisted of two TLR4–MD-2 heterodimers, six C16-sulfatide molecules, 61,898 TIP3P (60) water molecules, 120 Cl^-, and 146 Na^+. AMBER ff14SB (61) and GAFF (62) force fields were used to model proteins and the sulfatide, respectively. Antechamber (63) was applied to generate the residue topology of C16-sulfatide. The particle mesh Ewald method (64) was used to accurately calculate the electrostatic energies with the long-ranged correction being taken into account. The minimization and simulation protocols were described in our previous publication (65). All MD simulations were performed using the pmemd.cuda program in AMBER 2018 (66). In total, 1,000 evenly selected and all the 12,500 MD snapshots were applied to conduct MM-PBSA-WSAS binding free energy and MM-GBSA (mechanics-generalized Born surface area) (67) free energy decomposition analysis, respectively, as described in our previous publication (65). An internal program was applied to identify hotspot residues based on ligand–residue interaction energies from MM-GBSA free energy decomposition analysis.

Statistical Analysis. Data were analyzed using one- or two-way ANOVA with the appropriate multiple-comparison test, or with Student's *t* test wherever applicable. Differences with $P < 0.05$ were considered to be significant. All experiments were repeated at least twice.

Data Availability. The coordinates and structure factors of mouse TLR4–MD-2 in complex with C16-sulfatide reported in this article have been deposited in the Protein Data Bank under ID code 7MLM. All other data are available in the main text or *SI Appendix*.

ACKNOWLEDGMENTS. We thank the Structural Biology Lab at the University of Texas Southwestern Medical Center for organizing the Advanced Photon Source (APS) data collection trips. We are grateful to Dr. A. A. Herskovits for the femur and tibia bones of MyD88-deficient mice, and for the BMDMs extracted from TRIF-deficient mice. We are grateful to Dr. R. N. Apte for the femur and tibia bones of TLR4-deficient mice. We thank Dr. I. Ben-Dror for excellent technical help and for critical reading of the manuscript. This work was supported by NIH Grants AI125581 and AI100627 (to B.B.), Lyda Hill Foundation (B.B.), and Israel Cancer Association Grant 20180115 and Israel Science Foundation Grant 2142/20 (to T.Z.). M.A. was supported by a fellowship from the Ministry of Science of Israel. Results shown in this report are derived from work performed at Argonne National Laboratory, Structural Biology Center at the APS, under US Department of Energy, Office of Biological and Environmental Research Contract DE-AC02-06CH11357. Research reported in this publication was supported by the Office of the Director, NIH under Award S10OD025018.

1. I. Botos, D. M. Segal, D. R. Davies, The structural biology of Toll-like receptors. *Structure* **19**, 447–459 (2011).
2. U. Ohto *et al*., Toll-like receptor 9 contains two DNA binding sites that function cooperatively to promote receptor dimerization and activation. *Immunity* **48**, 649–658.e4 (2018).
3. L. Yu, L. Wang, S. Chen, Endogenous Toll-like receptor ligands and their biological significance. *J. Cell. Mol. Med.* **14**, 2592–2603 (2010).
4. K. A. Shirey *et al*., The TLR4 antagonist eritoran protects mice from lethal influenza infection. *Nature* **497**, 498–502 (2013).
5. B. Gao, M. F. Tsan, Recombinant human heat shock protein 60 does not induce the release of tumor necrosis factor alpha from murine macrophages. *J. Biol. Chem.* **278**, 22523–22529 (2003).
6. M. Manček-Keber, R. Jerala, Postulates for validating TLR4 agonists. *Eur. J. Immunol.* **45**, 356–370 (2015).
7. Y. Wang *et al*., Adjuvant effect of the novel TLR1/TLR2 agonist diprovocim synergizes with anti-PD-L1 to eliminate melanoma in mice. *Proc. Natl. Acad. Sci. U.S.A.* **115**, E8698–E8706 (2018).
8. Y. Wang *et al*., TLR4/MD-2 activation by a synthetic agonist with no similarity to LPS. *Proc. Natl. Acad. Sci. U.S.A.* **113**, E884–E893 (2016).
9. T. Takahashi, T. Suzuki, Role of sulfatide in normal and pathological cells and tissues. *J. Lipid Res.* **53**, 1437–1450 (2012).
10. A. A. Ilyas, Z. W. Chen, S. D. Cook, Antibodies to sulfatide in cerebrospinal fluid of patients with multiple sclerosis. *J. Neuroimmunol.* **139**, 76–80 (2003).
11. X. H. Zhu, A. Hara, T. Taketomi, The existence of galactosylceramide I_3-sulfate in serums of various mammals and its anticoagulant activity. *J. Biochem.* **110**, 241–245 (1991).
12. J. L. Kanter *et al*., Lipid microarrays identify key mediators of autoimmune brain inflammation. *Nat. Med.* **12**, 138–143 (2006).
13. C. Marsching *et al*., Renal sulfatides: Sphingoid base-dependent localization and region-specific compensation of CerS2-dysfunction. *J. Lipid Res.* **55**, 2354–2369 (2014).
14. A. L. Moyano *et al*., Levels of plasma sulfatides C18 : 0 and C24 : 1 correlate with disease status in relapsing-remitting multiple sclerosis. *J. Neurochem.* **127**, 600–604 (2013).
15. I. Maricic, R. Halder, F. Bischof, V. Kumar, Dendritic cells and anergic type I NKT cells play a crucial role in sulfatide-mediated immune regulation in experimental autoimmune encephalomyelitis. *J. Immunol.* **193**, 1035–1046 (2014).
16. A. Jahng *et al*., Prevention of autoimmunity by targeting a distinct, noninvariant CD1d-reactive T cell population reactive to sulfatide. *J. Exp. Med.* **199**, 947–957 (2004).
17. X. Han, D. M Holtzman, D. W. McKeel Jr, J. Kelley, J. C. Morris, Substantial sulfatide deficiency and ceramide elevation in very early Alzheimer's disease: Potential role in disease pathogenesis. *J. Neurochem.* **82**, 809–818 (2002).
18. K. Buschard, M. Blomqvist, T. Osterbye, P. Fredman, Involvement of sulfatide in beta cells and type 1 and type 2 diabetes. *Diabetologia* **48**, 1957–1962 (2005).
19. K. Buschard, K. Hanspers, P. Fredman, E. P. Reich, Treatment with sulfatide or its precursor, galactosylceramide, prevents diabetes in NOD mice. *Autoimmunity* **34**, 9–17 (2001).
20. G. Constantin, C. Laudanna, P. Baron, G. Berton, Sulfatides trigger cytokine gene expression and secretion in human monocytes. *FEBS Lett.* **350**, 66–70 (1994).
21. E. Altomare *et al*., Synthetic isoforms of endogenous sulfatides differently modulate indoleamine 2,3-dioxygenase in antigen presenting cells. *Life Sci.* **89**, 176–181 (2011).
22. H. Higashi *et al*., Intervention in endotoxin shock by sulfatide (I_3SO_3-GalCer) with a concomitant reduction in tumor necrosis factor alpha production. *Infect. Immun.* **65**, 1223–1227 (1997).
23. S. B. Jeon, H. J. Yoon, S. H. Park, I. H. Kim, E. J. Park, Sulfatide, a major lipid component of myelin sheath, activates inflammatory responses as an endogenous stimulator in brain-resident immune cells. *J. Immunol.* **181**, 8077–8087 (2008).
24. K. Buschard, J. E. Månsson, B. O. Roep, T. Nikolic, Self-glycolipids modulate dendritic cells changing the cytokine profiles of committed autoreactive T cells. *PLoS One* **7**, e52639 (2012).
25. H. S. Kim *et al*., Sulfatide inhibits HMGB1 secretion by hindering Toll-like receptor 4 localization within lipid rafts. *Front. Immunol.* **11**, 1305 (2020).
26. J. K. Ryu *et al*., Reconstruction of LPS transfer cascade reveals structural determinants within LBP, CD14, and TLR4-MD2 for efficient LPS recognition and transfer. *Immunity* **46**, 38–50 (2017).
27. E. Hailman *et al*., Lipopolysaccharide (LPS)-binding protein accelerates the binding of LPS to CD14. *J. Exp. Med.* **179**, 269–277 (1994).
28. J. Deguine, G. M. Barton, MyD88: A central player in innate immune signaling. *F1000Prime Rep.* **6**, 97 (2014).
29. M. Yamamoto *et al*., Role of adaptor TRIF in the MyD88-independent Toll-like receptor signaling pathway. *Science* **301**, 640–643 (2003).
30. K. Hoebe, B. Beutler, LPS, dsRNA and the interferon bridge to adaptive immune responses: Trif, Tram, and other TIR adaptor proteins. *J. Endotoxin Res.* **10**, 130–136 (2004).
31. J. Hambleton, S. L. Weinstein, L. Lem, A. L. DeFranco, Activation of c-Jun N-terminal kinase in bacterial lipopolysaccharide-stimulated macrophages. *Proc. Natl. Acad. Sci. U.S.A.* **93**, 2774–2778 (1996).
32. U. Ohto, K. Fukase, K. Miyake, T. Shimizu, Structural basis of species-specific endotoxin sensing by innate immune receptor TLR4/MD-2. *Proc. Natl. Acad. Sci. U.S.A.* **109**, 7421–7426 (2012).
33. A. S. Don *et al*., Altered lipid levels provide evidence for myelin dysfunction in multiple system atrophy. *Acta Neuropathol. Commun.* **2**, 150 (2014).
34. B. S. Park *et al*., The structural basis of lipopolysaccharide recognition by the TLR4-MD-2 complex. *Nature* **458**, 1191–1195 (2009).
35. U. Ohto, K. Fukase, K. Miyake, Y. Satow, Crystal structures of human MD-2 and its complex with antiendotoxic lipid IVa. *Science* **316**, 1632–1634 (2007).
36. H. M. Kim *et al*., Crystal structure of the TLR4-MD-2 complex with bound endotoxin antagonist eritoran. *Cell* **130**, 906–917 (2007).
37. T. Hou, J. Wang, Y. Li, W. Wang, Assessing the performance of the MM/PBSA and MM/GBSA methods. 1. The accuracy of binding free energy calculations based on molecular dynamics simulations. *J. Chem. Inf. Model.* **51**, 69–82 (2011).
38. Y. Kondo *et al*., TLR4-MD-2 complex is negatively regulated by an endogenous ligand, globotetraosylceramide. *Proc. Natl. Acad. Sci. U.S.A.* **110**, 4714–4719 (2013).
39. T. Nitta *et al*., Globo-series glycosphingolipids enhance Toll-like receptor 4-mediated inflammation and play a pathophysiological role in diabetic nephropathy. *Glycobiology* **29**, 260–268 (2019).
40. J. Meng, E. Lien, D. T. Golenbock, MD-2-mediated ionic interactions between lipid A and TLR4 are essential for receptor activation. *J. Biol. Chem.* **285**, 8695–8702 (2010).
41. B. W. Wattenberg, The long and the short of ceramides. *J. Biol. Chem.* **293**, 9922–9923 (2018).
42. M. Levy, A. H. Futerman, Mammalian ceramide synthases. *IUBMB Life* **62**, 347–356 (2010).
43. Y. Mizutani, A. Kihara, Y. Igarashi, Mammalian Lass6 and its related family members regulate synthesis of specific ceramides. *Biochem. J.* **390**, 263–271 (2005).
44. A. H. Futerman, H. Riezman, The ins and outs of sphingolipid synthesis. *Trends Cell Biol.* **15**, 312–318 (2005).
45. C. Marsching *et al*., Quantitative imaging mass spectrometry of renal sulfatides: Validation by classical mass spectrometric methods. *J. Lipid Res.* **55**, 2343–2353 (2014).
46. Y. Hirahara, R. Bansal, K. Honke, K. Ikenaka, Y. Wada, Sulfatide is a negative regulator of oligodendrocyte differentiation: Development in sulfatide-null mice. *Glia* **45**, 269–277 (2004).
47. I. Ishizuka, Chemistry and functional distribution of sulfoglycolipids. *Prog. Lipid Res.* **36**, 245–319 (1997).
48. Z. Pernber, M. Molander-Melin, C. H. Berthold, E. Hansson, P. Fredman, Expression of the myelin and oligodendrocyte progenitor marker sulfatide in neurons and astrocytes of adult rat brain. *J. Neurosci. Res.* **69**, 86–93 (2002).
49. Z. Berntson, E. Hansson, L. Rönnbäck, P. Fredman, Intracellular sulfatide expression in a subpopulation of astrocytes in primary cultures. *J. Neurosci. Res.* **52**, 559–568 (1998).
50. M. Wender, Z. Adamczewska, A. Zórawski, Fatty acid pattern of cerebral lipids in experimental allergic encephalomyelitis. *Z. Neurol.* **201**, 227–240 (1972).
51. R. L. Shaner *et al*., Quantitative analysis of sphingolipids for lipidomics using triple quadrupole and quadrupole linear ion trap mass spectrometers. *J. Lipid Res.* **50**, 1692–1707 (2009).
52. M. Mirzaian, G. Kramer, B. J. Poorthuis, Quantification of sulfatides and lysosulfatides in tissues and body fluids by liquid chromatography-tandem mass spectrometry. *J. Lipid Res.* **56**, 936–943 (2015).
53. M. Pizzuto *et al*., Saturation of acyl chains converts cardiolipin from an antagonist to an activator of Toll-like receptor-4. *Cell. Mol. Life Sci.* **76**, 3667–3678 (2019).
54. D. Avni, O. Ernst, A. Philosoph, T. Zor, Role of CREB in modulation of TNFalpha and IL-10 expression in LPS-stimulated RAW264.7 macrophages. *Mol. Immunol.* **47**, 1396–1403 (2010).
55. T. Zor, Z. Selinger, Linearization of the Bradford protein assay increases its sensitivity: Theoretical and experimental studies. *Anal. Biochem.* **236**, 302–308 (1996).
56. W. Minor, M. Cymborowski, Z. Otwinowski, M. Chruszcz, HKL-3000: The integration of data reduction and structure solution—From diffraction images to an initial model in minutes. *Acta Crystallogr. D Biol. Crystallogr.* **62**, 859–866 (2006).
57. A. J. McCoy, R. W. Grosse-Kunstleve, L. C. Storoni, R. J. Read, Likelihood-enhanced fast translation functions. *Acta Crystallogr. D Biol. Crystallogr.* **61**, 458–464 (2005).
58. P. Emsley, K. Cowtan, Coot: Model-building tools for molecular graphics. *Acta Crystallogr. D Biol. Crystallogr.* **60**, 2126–2132 (2004).
59. P. D. Adams *et al*., PHENIX: A comprehensive Python-based system for macromolecular structure solution. *Acta Crystallogr. D Biol. Crystallogr.* **66**, 213–221 (2010).
60. W. L. Jorgensen, J. Chandrasekhar, J. D. Madura, R. W. Impey, M. L. Klein, Comparison of simple potential functions for simulating liquid water. *J. Chem. Phys.* **79**, 926 (1983).
61. J. A. Maier *et al*., ff14SB: Improving the accuracy of protein side chain and backbone parameters from ff99SB. *J. Chem. Theory Comput.* **11**, 3696–3713 (2015).
62. J. Wang, R. M. Wolf, J. W. Caldwell, P. A. Kollman, D. A. Case, Development and testing of a general Amber force field. *J. Comput. Chem.* **25**, 1157–1174 (2004).
63. J. Wang, W. Wang, P. A. Kollman, D. A. Case, Automatic atom type and bond type perception in molecular mechanical calculations. *J. Mol. Graph. Model.* **25**, 247–260 (2006).
64. T. Darden, L. Perera, L. Li, L. Pedersen, New tricks for modelers from the crystallography toolkit: The particle mesh Ewald algorithm and its use in nucleic acid simulations. *Structure* **7**, R55–R60 (1999).
65. L. Su *et al*., Structural basis of TLR2/TLR1 activation by the synthetic agonist diprovocim. *J. Med. Chem.* **62**, 2938–2949 (2019).
66. D. A. Case *et al*., AMBER 2015 (University of California, San Francisco, 2015).
67. E. Wang *et al*., End-point binding free energy calculation with MM/PBSA and MM/GBSA: Strategies and applications in drug design. *Chem. Rev.* **119**, 9478–9508 (2019).